Supporting Information

Pablo Díaz-Núñez,[a] Sabrina L. J. Thomä,[b] Guillermo González-Rubio,[d] Olivia Borrell-Grueiro,[d,e] Roland P. M. Höller,[b,c] Munish Chanana,[b,f] David Garoz,[g] Luis Bañares,[d,h] Elena Junquera,[d] Andrés Guerrero-Martínez,[*d] Antonio Rivera,[*a,i] and Ovidio Peña-Rodríguez[*a,i]

[a]Instituto de Fusión Nuclear "Guillermo Velarde", Universidad Politécnica de Madrid, José Gutiérrez Abascal 2, E-28006 Madrid, Spain.

[b]University of Bayreuth, Department of Chemistry II, Universitätsstraße 30, D-95440 Bayreuth, Germany.

[c]Leibniz-Institut für Polymerforschung Dresden e.V., Institute of Physical Chemistry and Polymer Physics, Hohe Str. 6, 01069 Dresden, Germany.

[d]Departamento de Química Física, Universidad Complutense de Madrid, Avenida Complutense s/n, 28040 Madrid, Spain.

[e]INSTEC, Universidad de la Habana, Avenida Salvador Allende 1110, Habana 10400, 6163, Cuba.

[f]Swiss Wood Solutions AG, Überlandstr. 129, CH-8600, Dübendorf, Switzerland

[g]IMDEA Materials - Madrid Institute for Advanced Studies of Materials, c/Eric Kandel, 2, Parque Científico y Tecnológico|Tecnogetafe, 28906, Getafe, Madrid, Spain.

[h]Instituto Madrileño de Estudios Avanzados en Nanociencia (IMDEA Nanoscience), Cantoblanco, 28049 Madrid, Spain.

[i]Departamento de Ingeniería Energética, ETSII Industriales, Universidad Politécnica de Madrid, José Gutiérrez Abascal 2, E-28006 Madrid, Spain.

[*]Corresponding authors. Email: aguerrero@quim.ucm.es (A.G.-M.), antonio.rivera@upm.es (A.R.), ovidio.pena@upm.es (O.P.-R.).

Rod–sphere cluster irradiation with femtosecond laser pulses: Cut and paste at the nanoscale

Experimental methods

Spherical Au NPs with an approximate diameter of 15.5±3 nm were synthesized via the Turkevich reduction method [1]. They were subsequently coated with BSA via a ligand-exchange process [2]. 49 mL of a 0.1 M $HAuCl_4$ solution were heated to boiling under stirring; then, 2 mL of a 1 wt% citrate solution were added under stirring. The yellow solution immediately turned colorless and then the color slowly changed to greyish-blue and then wine red. After the color change was completed the heating was stopped. Cetylammoniumbromide (CTAB)-stabilized Au nanorods were synthesized using a process that we have described elsewhere [3–5]. They had a length of 63±7 nm, a diameter of 20±4 nm and an aspect ratio of 3.2±0.7.

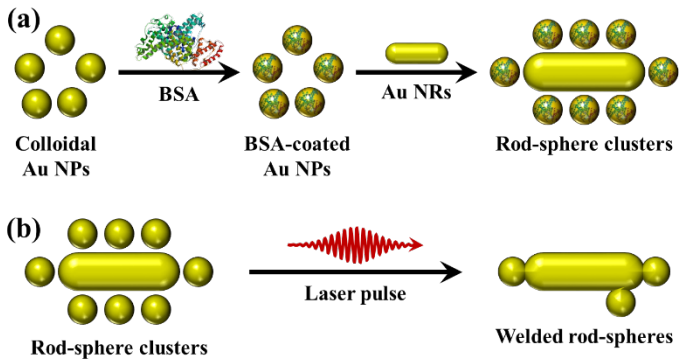

Figure S1. Schematic representation of (a) synthesis of Au rod-sphere nanoclusters and (b) welding of those nanoclusters by irradiation with fs laser pulses.

The core-satellite nanoclusters were obtained by adapting the protein-assisted assembly approach developed by Chanana et al. [6]. First, 5.5 mL of a BSA-citrate solution (1 mg/mL) was added to the nanoparticle dispersion and incubated overnight. Afterwards, the nanoparticle dispersion was purified to remove the excess of BSA by at least four cycles of centrifugation and redispersion (mini centrifuge 10500 rpm, 30 – 40 minutes). At the same time the nanoparticles were concentrated approximately 100-times. The nanoparticles were then redispersed, washed and stored in Milli-Q water at pH ~11. Next, rod-sphere nanoclusters were synthesized by adding the Au NRs to an excess of concentrated and purified BSA-coated Au spheres (Fig. S1a). Before addition, the Au NR dispersions were diluted ten times in Milli-Q water, to obtain a very low CTAC concentration (0.2 mM). After the synthesis the excess of spheres was removed by centrifugation.

In order to study the effects of laser irradiation over rod-sphere assemblies, suitable systems (assemblies with the plasmon band located around 800 nm) were irradiated with a Ti-sapphire NIR fs laser (wavelength 800 nm, pulse duration 50 fs, and repetition rate 1 kHz). The colloidal dispersions, all with similar optical density (~0.4) at 800 nm, were irradiated during 12 minutes, using laser fluences of 0.5, 1, 2, 4 and 6 J/m^2. Furthermore, we also performed an additional irradiation for 1 hour at the two lower fluences (0.5 and 1 J/m^2).

The optical properties of all colloidal dispersions (core rods, satellite particles and assemblies, before and after irradiation) were studied with UV-Vis spectroscopy. Spectra were acquired at room temperature with a Genesys 10S spectrophotometer in a wavelength range from 250 to 1100 nm. The shape and composition of all the nanostructures was investigated by transmission electron microscopy (TEM), using a JEM 1400 PLUS microscope with an accelerating voltage of 80 kV. For imaging, a 4 µL droplet of highly-concentrated NP dispersions was put on carbon-coated mesh copper grids and dried in air at room temperature. TEM images were used to determine the size distribution and morphology of the core and satellite nanoparticles as well as the composition of the nanoclusters.

Optical response of nanorod-nanosphere clusters

The optical response of nanorod-nanosphere cluster is studied by finite-differences in the time-domain (FDTD) using the free software computer code MEEP [7]. A detailed description of the FDTD method can be reviewed elsewhere [8,9].

Simulated geometries

The as synthesized and the irradiated structures exhibit diverse configurations, with the surrounding spheres at the tips and, also, along the length of the nanorod. To study these complex structures, several ideal configurations, represented and summarized in Figure S2 and Table S1, respectively, are considered. The simplest structures were simulated first: a NR with a NS next to each tip. Then, lateral NSs are added to the NR, equally distributed along its longitudinal axis to generate more complicated structures.

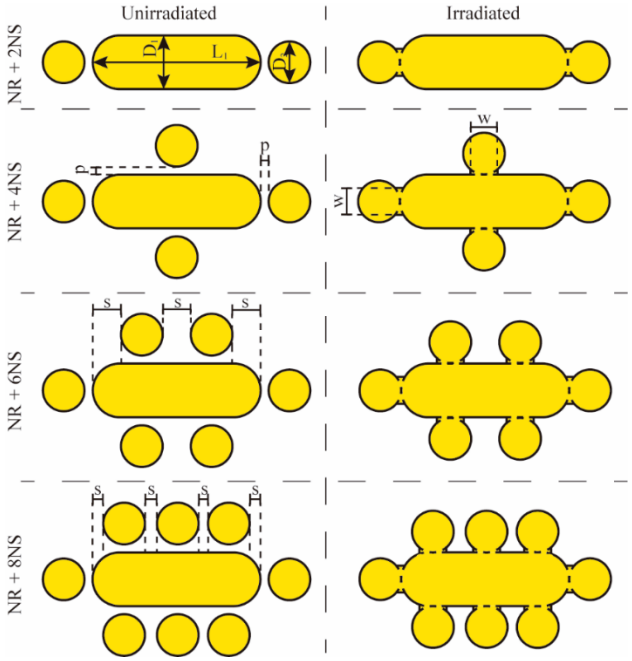

Figure S2: Simulated geometries for unirradiated (left) and irradiated (right) configurations with different number of nanospheres around the nanorod. The geometrical parameters are indicated in the figure: length of NR (L_1), width of NR (D_1), diameter of the external NS (D_2), distance between the external NS and the NR (p), distance between external NS (s) and diameter of junction (w).

	Structure	L1 (nm)	D1 (nm)	D2 (nm)	S (nm)	P (nm)	W (nm)
Unirradiated	NR + 2NS	62. 5	20.0	15.5	-	3	-
	NR + 4NS	62. 5	20.0	15.5	-	3	-
	NR + 6NS	62. 5	20.0	15.5	10.5	3	-
	NR + 8NS	62. 5	20.0	15.5	4	3	-
Irradiated	NR + 2NS	62. 5	20.0	15.5	-	0	10
	NR + 4NS	62. 5	20.0	15.5	-	0	10
	NR + 6NS	62. 5	20.0	15.5	10.5	0	10
	NR + 8NS	62. 5	20.0	15.5	4	0	10

Table S1: Dimension of the configurations described in Figure S2.

The NR is constructed as a hemispherically capped cylinder with a length (L_1) of 62.5 nm and a width of (D_1) of 20 nm and the diameter of the external (D_2) spheres is 15.5 nm. These values are applied for all the structures. The distance between the external NS and the NR (p) is 3 nm for the unirradiated structures and 0 for the irradiated structures. The gap between the lateral external spheres (s) is 10.5 and 4 nm for the configurations with 6 and 8 spheres, respectively. The junction between the external NS and the NR for the irradiated structures in simplified as a cylinder width a diameter (w) of 10 nm. Table 1 summarized the simulated structures.

Computational cell

The computational cell size is $(4D_1+8p+8D_2)\times(4D_1+8p+8D_2)\times(4D_1+8p+8D_2)$ nm^3 with a spatial resolution of 0.5 nm. The cell is surrounded by perfectly matched layers (PML, represented by the diagonal lined area in Figure 2) with a thickness of D_1 to absorb the scattered waves. The structure is placed at the center of the simulation box, with the lateral NS placed in the *XY* plane. A broadband Gaussian source is placed at the top of the cell and the EM wave propagated along the *Z* direction. The fields are allowed to evolve, and the simulation is terminated once $|\mathbf{E}|^2/|\mathbf{E}_{max}|^2$ decays down to 10^{-8} at the bottom of the cell in the Z direction. The refractive index of the surrounding medium was fixed at 1.395 to account the presence of the protein coating [10]. The permittivity function of gold is modelled using a Drude term and five Lorentzians [11].

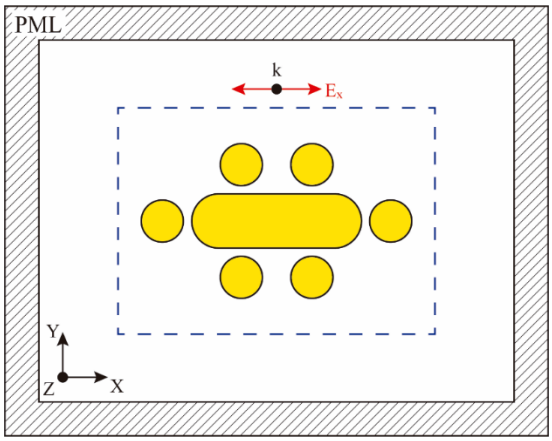

Figure S3: Schematic representation of the simulation cell used in the FDTD simulations. The surrounding area represents the perfectly matched layers, used to absorb the scattered waves. The dashed blue lines represent the areas where the integral of the Poynting vector is applied to calculate the incident, absorbed and scattered power. The simulation was performed for parallel polarized light, propagating along the Z direction. The external NSs are placed in the XY plane. The simulation is terminated once the electric fields have decayed sufficiently.

The optical response in the far field is analyzed by means of the optical extinction efficiency factor (Q_{ext}). The value of Q_{ext} is calculated from the extinction cross section (C_{ext}) and the cross-sectional area of the structure projected onto a plane perpendicular to the incident light (A) using the following equation [12]:

$$Q_{ext} = \frac{C_{ext}}{A} \quad (2)$$

The extinction cross section represents the rate at which the incident radiation, I_{inc}, is attenuated by the structure and, in a non-absorbing medium, it is calculated as the sum of the absorption (C_{abs}) and scattering (C_{sca}) cross sections [12]:

$$C_{ext} = C_{abs} + C_{sca} = \frac{W_{abs}+W_{sca}}{I_{inc}} \quad (3)$$

In equation 3, W_{abs} and W_{sca} are the absorbed and scattered power by the structure, respectively. The values of W_{abs} and W_{sca} are calculated as the integral of the Poynting vector of the Fourier-transformed electric and

magnetic fields at each frequency (ω) over a closed area around the structure (this area is represented as the blue dashed line around the particle in Figure S3) to obtain a full spectrum in a single simulation [7]:

$$W(\omega) = \Re \oiint \mathbf{E}_\omega \times \mathbf{H}_\omega d\mathbf{S} \qquad (4).$$

For calculating I_{inc}, the same expression is applied but only for an area perpendicular to the direction of propagation of the wave in an empty simulation cell, *i.e.,* without the structure. The simulation is performed thrice to calculate the incident, absorbed and scattered power in each run.

Finally, the near-field response is evaluated by means of the field enhancement, $|\mathbf{E}|/|\mathbf{E}_0|$. Each component of the complex electric field (E_x, E_y and E_z) is stored at each time step and every point of the space in the simulation cell. Once the fields, which are of the form of $\mathbf{E} = \mathbf{E}(x, y, z, t)$, have been accumulated over the full simulation time, they are Fourier-transformed to obtain a full spectrum of the electric fields in the frequency domain, $\mathbf{E} = \mathbf{E}(x, y, z, \omega)$, for all the space considered in the simulation cell. This calculation is performed twice: with the structure to obtain scattered fields, $|\mathbf{E}|$ and without the structure to obtain the incident fields, $|\mathbf{E}_0|$, to normalize the previous result.

A typical result of these calculations is shown in Figure **S4**, to illustrate the split of the main plasmon band, due to the plasmonic modes that appear in the new structure.

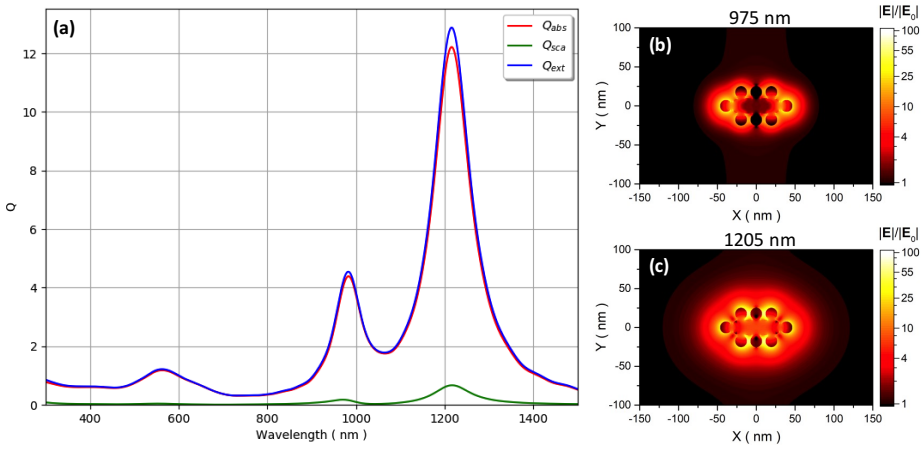

Figure S4: (a) Simulated efficiencies calculated for a nanorod surrounded by eight satellite spheres. The color maps represent the near-field distribution of the electric field at the wavelengths of (b) 975 nm and (c) 1205 nm.

Thermal calculation

The thermal cooling of the gold nanoparticle and nearby spheres has been calculated with a continuum model based on finite elements. The axisymmetric geometry with vertical symmetry represents one nanoparticle (rod) and two spheres close to each end of the rod (Figure S5). Nanoparticle and spheres are into a finite domain, which represents the water or the vacuum in different scenarios. The thermal properties for gold and water were taken from Ekici et al. [13]. The initial conditions are the temperature of the rod, sphere and water. The adiabatic conditions on the axisymmetric and symmetric edges are complemented with a fixed temperature on the external edges of the water domain at 300 K. The discretized model with heat transfer elements has been solved with an implicit solver under quasi-static conditions. Two main scenarios are distinguished: one model with the rod and sphere separated 2 nm; and the other one where rod and sphere are touching each other (the radius of the contact area is 1 nm). In both cases the initial temperature of the rod and sphere were 1915 K and 703 K, respectively. When rod and sphere are separated 2 nm, the temperature of both decreases until room temperature in a characteristic time of 1 ns. When the sphere is touching the rod, the high thermal conductivity of the metal equilibrates the initial temperatures at 1420 K in just 20 ps, then the cooling of the metal reaches the room temperature in the range of nanoseconds.

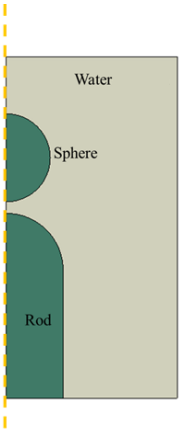

Figure S5: Schematic representation of the simulation cell used in the Finite Elements simulations.

Bibliography

1. J. Turkevich, P. C. Stevenson, and J. Hillier, "A study of the nucleation and growth processes in the synthesis of colloidal gold," Discuss. Faraday Soc. **11**, 55–75 (1951).
2. M. Chanana, P. Rivera_Gil, M. A. Correa- Duarte, L. M. Liz- Marzán, and W. J. Parak, "Physicochemical properties of protein-coated gold nanoparticles in biological fluids and cells before and after proteolytic digestion," Angew. Chem. Int. Ed. **52**, 4179–4183 (2013).
3. G. González-Rubio, J. González-Izquierdo, L. Bañares, G. Tardajos, A. Rivera, T. Altantzis, S. Bals, O. Peña-Rodríguez, A. Guerrero-Martínez, and L. M. Liz-Marzan, "Femtosecond laser-controlled tip-to-tip assembly and welding of gold nanorods," Nano Lett. **15**, 8282–8288 (2015).
4. G. González-Rubio, P. Díaz-Núñez, A. Rivera, A. Prada, G. Tardajos, J. González-Izquierdo, L. Bañares, P. Llombart, L. G. Macdowell, M. A. Palafox, L. M. Liz-Marzán, O. Peña-Rodríguez, and A. Guerrero-Martínez, "Femtosecond laser reshaping yields gold nanorods with ultranarrow surface plasmon resonances," Science **358**, 640–644 (2017).
5. P. Díaz-Nuñez, G. González-Rubio, A. Prada, J. González Izquierdo, A. Rivera, L. Bañares, A. Guerrero-Martínez, and O. Peña-Rodríguez, "Using femtosecond laser irradiation to grow the belly of gold nanorods," J. Phys. Chem. C **122**, 19816–19822 (2018).
6. R. P. M. Höller, M. Dulle, S. Thomä, M. Mayer, A. M. Steiner, S. Förster, A. Fery, C. Kuttner, and M. Chanana, "Protein-assisted assembly of modular 3D plasmonic raspberry-like core/satellite nanoclusters: Correlation of structure and optical properties," ACS Nano **10**, 5740–5750 (2016).
7. A. F. Oskooi, D. Roundy, M. Ibanescu, P. Bermel, J. D. Joannopoulos, and S. G. Johnson, "Meep: A flexible free-software package for electromagnetic simulations by the FDTD method," Comput. Phys. Commun. **181**, 687–702 (2010).
8. A. Taflove and S. C. Hagness, *Computational Electrodynamics: The Finite-Difference Time-Domain Method.*, 3rd ed. (Artech House, 2005).
9. A. Taflove, A. F. Oskooi, and S. G. Johnson, *Advances in FDTD Computational Electrodynamics: Photonics and Nanotechnology* (Artech House, 2013).
10. R. P. M. Höller, M. Dulle, S. Thomä, M. Mayer, A. M. Steiner, S. Förster, A. Fery, C. Kuttner, and M. Chanana, "Protein-Assisted Assembly of Modular 3D Plasmonic Raspberry-like Core/Satellite Nanoclusters: Correlation of Structure and Optical Properties," ACS Nano **10**, 5740–5750 (2016).
11. A. D. Rakić, A. B. Djurišić, J. M. Elazar, and M. L. Majewski, "Optical properties of metallic films for vertical-cavity optoelectronic devices," Appl. Opt. **37**, 5271–5283 (1998).
12. C. F. Bohren and D. R. Huffman, eds., *Absorption and Scattering of Light by Small Particles* (Wiley-VCH Verlag GmbH, 1998).
13. O. Ekici, R. K. Harrison, N. J. Durr, D. S. Eversole, M. Lee, and A. Ben-Yakar, "Thermal analysis of gold nanorods heated with femtosecond laser pulses," J. Phys. Appl. Phys. **41**, 185501 (2008).